**Steel and Composite Structures**, *Vol. 35, No. 3 (2020) 353-370*
DOI: https://doi.org/10.12989/scs.2020.35.3.353


# A new replaceable fuse for moment resisting frames: Replaceable bolted reduced beam section connections

Yasin O. Özkılıç*

*Department of Civil Engineering, Necmettin Erbakan University, 42100, Konya, Turkey*

(*Received October 23, 2019, Revised February 21, 2020, Accepted April 13, 2020*)

**Abstract.** This paper describes a new type of replaceable fuse for moment resisting frames. Column-tree connections with beam splice connections are frequently preferred in the moment resisting frames since they eliminate field welding and provide good quality. In the column-tree connections, a part of the beam is welded to the column in the shop and the rest of the beam is bolted with the splice connection in the field. In this study, a replaceable reduced beam section (R-RBS) connection is proposed in order to eliminate welding process and facilitate assembly at the site. In the proposed R-RBS connection, one end is connected by a beam splice connection to the beam and the other end is connected by a bolted end-plate connection to the column. More importantly is that the proposed R-RBS connection allows the replacement of the damaged R-RBS easily right after an earthquake. Pursuant to this goal, experimental and numerical studies have been undertaken to investigate the performance of the R-RBS connection. An experimental study on the RBS connection was used to substantiate the numerical model using ABAQUS, a commercially available finite element software. Additionally, five different finite element models were developed to conduct a parametric study. The results of the analysis were compared in terms of the moment and energy absorption capacities, PEEQ, rupture and tri-axiality indexes. The design process as well as the optimum dimensions of the R-RBS connections are presented. It was also demonstrated that the proposed R-RBS connection satisfies AISC criteria based on the nonlinear finite element analysis results.

**Keywords:** reduced beam section; ABAQUS; rupture index; PEEQ; column-tree connections; cyclic loading; beam splice; tri-axiality index; replaceable fuse

## 1. Introduction

Moment resisting frames (MRFs) are extensively used as lateral load resisting systems where large openings are required. Welded flange and bolted web connections were commonly preferred in MRFs before the Northridge, 1994 and Kobe, 1995 earthquakes. After these earthquakes, brittle failures were observed at beam-to-column connections which led the researchers to investigate the reason of the failures. Poor workmanship and inadequate welding process were among the main reasons of these failures (Shen 2009). In order to prevent these failures, two possible solutions were mainly proposed to shift the plastic hinge away from the column face: increasing the capacity of the connection and the column or decreasing the capacity of the beam. The reduced beam section (RBS) connection is a weakening method based on a deliberate reduction of the beam capacity by reducing the flange section area to let the development of the plastic deformation at a predefined beam section. The RBS connection is a widely used method in MFRs (Shen 2009). The idea of RBS connection was first stated in the research conducted by Plumier (1997). Various cutout shapes for RBS connections such as tapered cut, radius cut, constant cut and drilled flange have been developed (Sophianopoulos and Deri 2011).

Swati and Gaurang (2014) investigated the behavior of moment connections with and without an RBS connection. They compared the results of the experimental and numerical studies and indicated that seismic performance of a beam with an RBS connection was better than that without an RBS connection. Pachoumis *et al.* (2009) conducted experimental and analytical studies in order to investigate the behavior of a radius cut RBS connection using HEA profiles. Pachoumis *et al.* (2010) tested two RBS connections under cyclic loading in order to examine the effectiveness of the parameters given in Eurocode 8. They recommended some modifications for the parameters of the RBS connection in Eurocode 8.

Oh *et al.* (2015, 2016) studied seismic performance of the RBS connection connected to the weak axis of the column-tree moment connections. The experimental studies showed that the beams with the RBS connections have more ductile and stable behavior compared to stub beams. In some cases, the RBS connection is obtained by trimming of the web. The seismic performance of the reduced web section (RWS) connection was analyzed using a nonlinear finite element (FE) model (Akrami and Erfani 2015, Momenzadeh *et al.* 2017, Zahrai *et al.* 2017a). The results indicated that the RWS connection enhances the behavior of the moment resisting frames. Zahrai *et al.* (2017b) performed both experimental and numerical studies to examine the behavior of tubular web RBS connections.

*Corresponding author, Research Assistant
E-mail: yoozkilic@gmail.com


http://www.techno-press.org/?journal=scs&subpage=8
ISSN: 1229-9367 (Print), 1598-6233 (Online)

Saleh *et al.* (2016) conducted three experiments under cyclic loading to investigate a novel tubular web RBS connection. Several studies were conducted in order to improve the behavior of the RBS connection. Roudsari *et al.* (2015, 2018) performed numerical and experimental studies to enhance the performance of the RBS connection by using stiffeners. Morshedi *et al.* (2017) proposed using a double radius cut adjacent to each other. Numerical analyses demonstrated that a double reduced beam section connection enhances the behavior of the RBS connection.

Zareia *et al.* (2016) conducted a numerical study using ABAQUS in order to investigate the behavior of the RBS connection under skewed condition. It was concluded that RBS connection is the best choice for the beam-to-column connection in the skewed condition. Oh *et al.* (2014) conducted experimental studies in order to investigate the seismic performance of the column-tree moment connection with a weakened beam splice. Sophianopoulos and Deri (2011) recommended combining the RBS connection with the extended end-plated connection. Sofias *et al.* (2014) studied the RBS connection with extended bolted end-plated connection experimentally and the specimens performed an excellent seismic performance under cyclic loading. In the present study, the end-plated connection is combined with the beam splice connection in order to facilitate the construction and allow the easy replacement of the RBS connection after an earthquake. In order to evaluate the performance of the proposed connection, the obtained response indices were utilized to assess the performance of the RBS connections. Similar approach was conducted to evaluate the RBS connections by many researchers (Atashzaban *et al*. 2015, Rahnavard *et al*. 2015, Xu *et al.* 2018)

The replaceable link concept was extensively used in eccentrically braced frames (EBFs) as well as in MRFs. For EBFs, the first practical replaceable link that can be easily replaceable after an earthquake was proposed in the study of Stratan and Dubina (2004) (Kazemzadeh Azad and Topkaya 2017). Later, Dubina and Stratan (2008) conducted an experimental program to investigate the seismic performance of the replaceable link with flush end-plated connection in EBFs. Various designs of the replaceable link for EBFs were proposed by many researchers (Mansur *et al.* 2011, Bozkurt and Topkaya 2017, 2018, Bozkurt *et al*. 2019).

The first replaceable link for MRFs was proposed by Balut and Gioncu (2003). A dog bone solution with bolted end-plated I-beam and bolted web connection with two channel sections were proposed. Later Shen *et al.* (2010) conducted four full-scale tests to examine the performance of the replaceable links for MRFs which were proposed by Balut and Gioncu (2003). The links with end-plated connection and back-to-back double channels were investigated experimentally and numerically in detail. The experimental results revealed that all specimens performed a good seismic response and the replaceable link with the end-plated connection dissipated a higher energy than that of the link with back-to-back double channels.

Nikoukalama and Dolatshahi (2015) proposed replaceable shear links for MRFs. The performance of the proposed links were studied under cycling loading numerically by finite element models using ABAQUS software. The results showed that the proposed links exhibited a higher ductility. Later, Mahmoudi *et al.* (2019) carried out an experimental program to investigate and verify the performance of the replaceable shear links previously proposed by Nikoukalama and Dolatshahi (2015). The experimental study proved that the proposed links can be a viable alternative to MRFs. Richards (2019) developed an innovative replaceable connection for MRFs and conducted two experiments to examine the seismic performance of the proposed replaceable connection. The connection performed a successful hysteresis behavior. Garoosi *et al.* (2019) conducted experimental and numerical studies in order to investigate the RBS connection as replaceable fuses. In their study, the RBS connection was attached to both the beam and column using an end-plated connection.

RBS connections are mostly used in the column-tree moment connections. A part of the beam is welded to the column in the shop and the rest of the beam is attached with a splice connection in the field. During a severe earthquake, it is expected that visible damages might occur at the RBS connection. Under severe earthquakes, however, even if no visible damages such as buckling of the web and flange have occurred, the RBS connection should still be replaced since it is too difficult to assess the level of damage occurred. Moreover, the damage can accumulate under several moderate or low level earthquakes. Therefore, replacing the RBS connection is preferred rather than evaluating the damage to see whether the beam can sustain another earthquake and provide sufficient safety. After an earthquake, when a replaceable connection is not used, the damaged beam must be cut with flame in order to be removed and the new beam replacement should be welded at the site. These processes require intensive labor and time. On the other hand, many damages have been reported due to improper welding. It was also reported that replacement of the damaged beam is very costly, problematic and time consuming for MRFs (Mahmoudi *et al*. 2019). The building cannot deliver services during maintenance, which leads additional burden to the owners in terms of money and time. In order to overcome these problems, R-RBS connection was proposed by Özkılıç (2019).

## 2. Replaceable reduced beam section connection

In this study, the RBS connection was utilized as a replaceable fuse for MRFs. In this present study, the R-RBS connection was separated from the column using a bolted end-plated connection and it was separated from the beam using a bolted beam splice connection. Fig. 1 shows the detail of the proposed replaceable RBS connection. The use of bolted end-plated connection together with the bolted beam splice connection can isolate the RBS connection from the entire beam and column so that only a small portion of the beam which is the RBS connection will be replaced using bolted connections which facilitates the replacement operation after an earthquake. Additionally, the

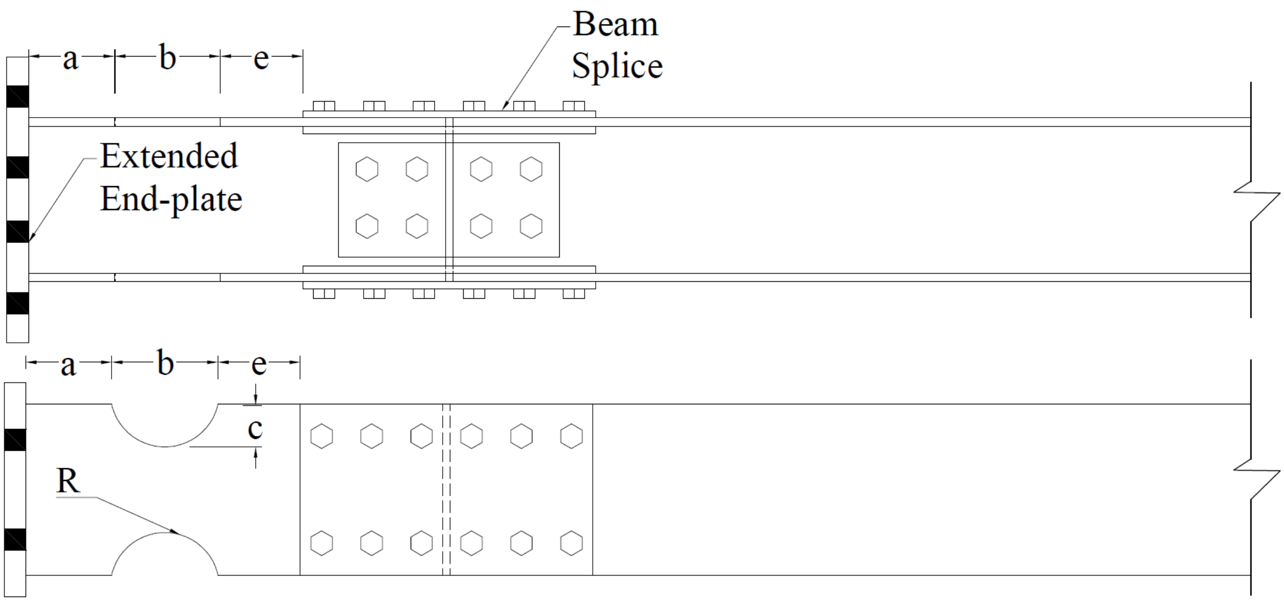


Fig. 1 The details of proposed connection and definition of the parameters

replaceable RBS connection will facilitate the assembly by allowing non-exact member dimensions by means of bolt hole tolerance.

### 2.1 Parameters for reduced beam section connection

The AISC provision (AISC, 2016a) limits the parameters *a*, *b* and *c* in order to ensure the plastic hinge to be formed at the radius cut section. The definition of these parameters are described in Fig. 1. It should be noted that these limitations are only valid for the radius cut section. Additionally, in this study, the parameter *e* is defined as the distance from the end of the radius cut section to the beam splice connection.

The limitations of these parameters are defined in the AISC provision and given in Eqs. (1)-(3)

$$0.5b_f \le a \le 0.75b_f \tag{1}$$

$$0.65d \le b \le 0.85d \tag{2}$$

$$0.1b_f \le c \le 0.25b_f \tag{3}$$

where $a$ is the horizontal distance from the face of column flange to the start of an RBS cut, $b$ is the length of RBS cut, $c$ is the depth of the cut at center of RBS, $d$ is the section d epth, $b_f$ is the flange width, $t_w$ and $t_f$ are the thickness of the web and flange, respectively.

### 2.2 The design of the end-plated connection for the RBS connection

The design of the end-plated connection for the RBS connections was performed according to the US practices. Two approaches are available in the US practices for the design of end plate connections which are thin plate design and thick plate design. If no prying forces are available, the plate is called as a thick plate and if the prying forces are maximum, then it is called as a thin plate. However, under seismic and wind conditions, the AISC358-18 (AISC, 2018) permits only to use thick plates for the design of the end plates. The *Design Guide 04: Extended End-Plate Moment Connections Seismic and Wind Applications* prepared by Murray and Summer (2003) explains the design of thick end plate, except that it adopts different resistance factors from the factors of the current version of the AISC provision (AISC, 2018). This guideline provides a step by step design procedure. In this study, four-bolt unstiffened extended end-plate connection was selected. According to AISC358-18 (AISC, 2018), the required end plate thickness and bolt diameter are determined from the Eqs. (4) and (5), respectively.

$$t_{p,reqd} = \sqrt{\frac{1.11M_f}{F_{py}Y}} \tag{4}$$

$$d_{p,reqd} = \sqrt{\frac{2M_f}{\pi\phi_n F_{nt}(h_0 + h_1)}} \tag{5}$$

where $M_f$ is the moment at the face of the column, $F_{py}$ is yield strength of the end plate, $Y$ is the yield-line mechanism parameter, $F_{nt}$ is nominal tensile strength of bolt, $h_o$ is the distance from the centerline of the compression flange to the tension side outer bolt row, $h_i$ is the distance from the centerline of the compression flange to the tension side inner bolt row and $\phi_n$=0.9. The calculation of the yield line parameter can be found in the AISC provision (AISC, 2016a). It is important that $M_f$ should be computed according to the capacity of the RBS connection and it is given in Eq. (6).

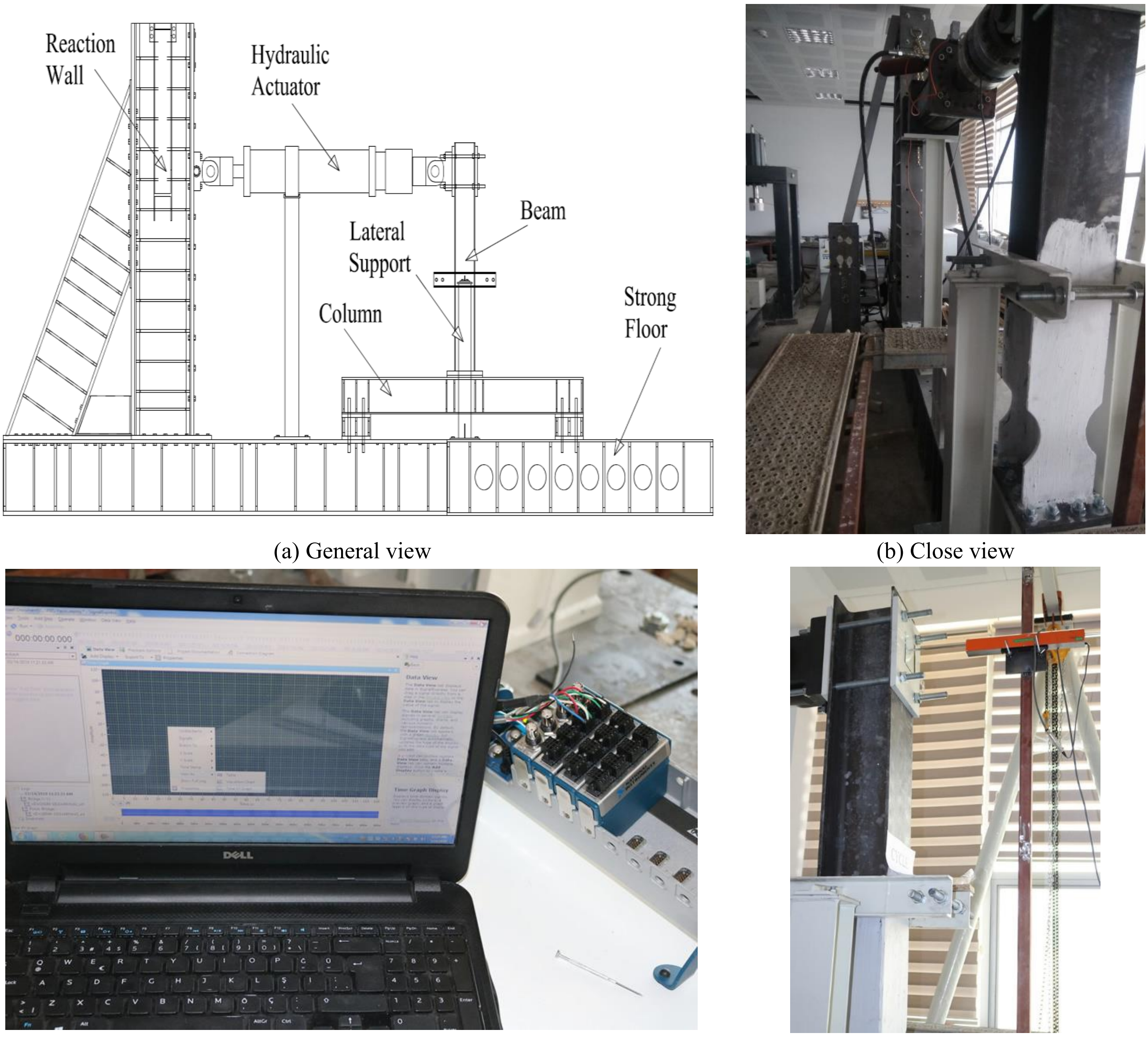


(a) General view (b) Close view

(c) Data acquisition (d) The location of LVDT

Fig. 2 Experimental setup

$$M_f = M_{pr} + V_{RBS} S_h \tag{6}$$

where $M_{pr}$ is the probable maximum moment at the plastic hinge, $S_h$ is the distance from the face of column to the plastic hinge, $V_{RBS}$ is the shear force at the end of beam. $S_h$ and $M_{pr}$ are calculated from Eqs. (7) and (8), respectively.

$$S_h = a + b/2 \tag{7}$$

$$M_{pr} = C_{pr} R_y F_y Z_{RBS} \tag{8}$$

where $C_{pr}$ is the factor to account for peak connection strength, including strain hardening, local restraint, additional reinforcement, and other connection conditions, $R_y$ is the ratio of the expected yield stress to the specified minimum yield stress, $Z_{RBS}$ is the plastic section modulus at the center of the reduced beam section. $C_{pr}$ and $Z_{RBS}$ can be calculated from Eqs. (9) and (10), respectively.

$$Z_{RBS} = Z_x - 2ct_f(d - t_f) \tag{9}$$

$$C_{pr} = \frac{F_y + F_u}{F_y} \leq 1.2 \tag{10}$$

where $Z_x$ is the plastic section modulus about x-axis for full beam cross section.

### *2.3 The design of the beam splice connection for RBS connection*

Table 1 Nominal and measured dimensions of RBS connection

| a (mm) | | b (mm) | | c (mm) | | R (mm) | |
|---|---|---|---|---|---|---|---|
| Nominal | Measured | Nominal | Measured | Nominal | Measured | Nominal | Measured |
| 152 | 151.7 | 66 | 65.8 | 45 | 44.8 | 34.6 | 34.5 |

Table 2 Nominal and measured dimensions of HEA240 section

| d (mm) | | $b_f$ (mm) | | $t_w$ (mm) | | $t_f$ (mm) | |
|---|---|---|---|---|---|---|---|
| Nominal | Measured | Nominal | Measured | Nominal | Measured | Nominal | Measured |
| 230 | 231.2 | 240 | 240.1 | 7.5 | 7.9 | 12 | 11.7 |

In the practice, the beam splice connections are designed as a rigid connection in the column-tree connections (Oh *et al.* 2014). Similar approach was used in the design of the R-RBS connection to avoid any damage being occurred at the beam splice connection so that the R-RBS connection can be easily replaceable after an earthquake. Therefore, the beam splice connection should be designed to be stronger than the capacity of the RBS connection. In the present study, the slip-critical connection was used and the bolts were fully pre-tensioned, which was recommend by the AISC (AISC, 2016a).

Numerical and experimental studies have been undertaken to examine the performance of the R-RBS connections. In order to investigate the behavior of the R-RBS connection in the MRFs, five FE models were developed in ABAQUS environment after verifying the numerical model against the experimental study. Following sections describe the experimental and numerical studies.

## 3. Material and methods

### *3.1 Experimental study*

Experimental study was carried out at Necmettin Erbakan University, Civil Engineering Department, Structural Engineering Laboratory. The aim of the experimental study was to provide experimental data for verification of the numerical model and also to examine the behavior of the RBS connection. The servo-controlled hydraulic actuator having capacity of 1000kN in compression and 600kN in tension was connected to the steel reaction wall. The lateral restraining system was assembled on the steel strong floor. Due to the position of the reaction wall and the hydraulic actuator, the column was placed horizontally to the steel strong floor so that the top of the beam was connected to the hydraulic actuator. The test specimen, which was designed according to AISC 2016 seismic provisions (AISC, 2016b), was assembled to the column with the bolted end-plated connection. The specimen was whitewashed in order to observe yielding pattern. The experimental setup including the reaction wall, strong floor, hydraulic actuator, lateral support, column and beam is depicted in Fig. 2.

Hot rolled I sections of HEB340 and HEA240 sections were selected as the column and beam, respectively. These sections were determined based on the restriction of the laboratory such as the capacity of the hydraulic actuator, the strong floor and the lateral support system. The column section was designed to behave elastic during the experiments. Table 1 demonstrates nominal and measured dimensions of the RBS connection while Table 2 provides the nominal and measured dimensions of properties of the ordered HEA240 section.

During the experiment, loading and displacements were recorded by both internal data acquisition of the hydraulic actuator and external National Instruments Data Acquisition System (Fig. 2(c)). Fig. 2(d) illustrates the connection of the hydraulic actuator to the beam and the location of Linear Variable Differential Transformer (LVDT). The LVDT with capacity of 300 mm was mounted 1650 mm above the column flange.

The test specimen was exposed to cyclic loading according to the AISC 2016 seismic provisions (AISC, 2016b). Six cycles were repeated at 0.00375rad, 0.005rad, and 0.0075rad, then four cycles were repeated at 0.01rad, later two cycles were repeated at 0.015rad and 0.02 rad. Following cycles were repeated two times with increments of 0.01 rad. The loading protocol is presented at Fig. 3. A beam should complete 0.04 rad and sustain a moment at the column face above 0.8 times the moment capacity of the beam in order to satisfy AISC criteria.

Three coupons and two coupons were extracted from the web and flanges respectively in order to measure material properties of the HEA240 section. Fig. 4(a) shows the coupon specimens and test setup. The results of each coupon test in terms of yield strain and modulus of elasticity are given in Table 3. The average yield stress of web and flanges are 320 MPa and 300 MPa, respectively. Fig. 4(b) demonstrates the average stress-strain curves of web and flanges. The end-plated connection in the experiment was intentionally over-designed to ensure no plastic deformation to be occurred in the end-plate. In the experiment, 30 mm thick end-plate and 20 M24 bolts with 10.9 grade were used. 26 mm bolt holes were drilled on the end-plate. According to AISC design explained in previous section, 25 mm thick end- plate and 8 M24 with 10.9 grade bolts were required. The beam splice was designed as slip-critical condition and stronger than the RBS connection.

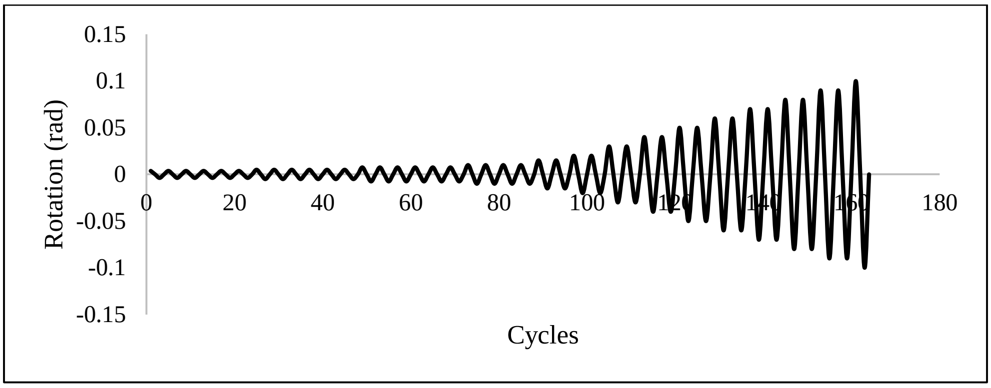


Fig. 3 AISC Loading Protocol (AISC, 2016b)

Coupon Test

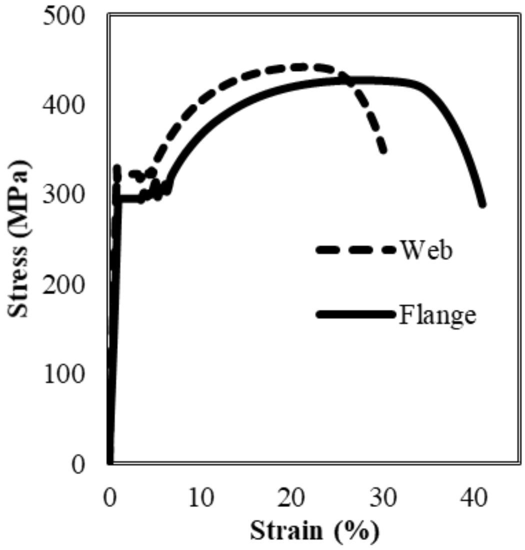


Strain-Stress Curves

Fig. 4 Coupon Test and Strain-Stress Curves

Table 3 The results of coupon tests

| | Web | | Flange | |
|---|---|---|---|---|
| Coupon | E (GPa) | $F_y$ (MPa) | E (GPa) | $F_y$ (MPa) |
| 1 | 194.45 | 314.79 | 201.82 | 299.87 |
| 2 | 204.55 | 327.65 | 199.32 | 302.46 |
| 3 | 199.32 | 318.12 | - | - |
| Average | 199.44 | 320.18 | 200.57 | 300.16 |

### *3.2 Numerical study*

The use of finite element analysis to solve complicated engineering problems has been increasing since last decade thanks to advancement in computer technology which enables to figure out advanced numerical calculations. Finite element analysis is an alternative way of experimental study which can be very exhausting and costly. In this present study, numerical models were generated utilizing ABAQUS finite element program in order to investigate the performance of the R-RBS connections. ABAQUS/Standard with version of 6.12-1 was used to simulate the experiment and to conduct a parametric study. ABAQUS is a quite reliable finite element program used by many researchers (Aghaei *et al*. 2015, Ashakul and Khampa 2014, Kazemzadeh Azad and Uy 2020, Chegenizadeh *et al.* 2014, Ding *et al.* 2017, Eom *et al.* 2019, Dere 2016, Kantar and Anil 2012, Kota *et al.* 2019, Lopez-Arancibia *et al.* 2015, Metwally 2014, Pantò *et al.* 2017, Wang *et al.* 2015, Song *et al.* 2019, Madenci *et al*. 2020, Özkılıç *et al*. 2020) to solve civil engineering problems.

Frictional contact surfaces are more prone to cause convergence problems and they also increase computational time significantly. Therefore, the column and its connections to the strong floor, and the lateral restraining system were not modeled explicitly. Instead, only the beam section and its connections were modeled in order to reduce computational time and eliminate any possible convergence problems. Moreover, proper mesh detailing should be employed around the bolt holes to reduce convergence problems.

Instead of modeling welding explicitly, tie constrain was used in the numerical models. Geometric nonlinearity was implemented using NIgeom option in ABAQUS to account large displacements and deformations. Initial imperfections were defined to simulate the buckling of the RBS connections after buckling analyses have been conducted.
According to the Author's best knowledge, two practical ways are available to give pretension force to the bolts in ABAQUS. Either Bolt Load option or temperature method can be used to apply the pretension. In this study, Bolt Load option was utilized to apply the pretensioning force. Each bolts was exposed to the pretensioning force according to the AISC 2016 specification for structural steel buildings (AISC, 2016c), for instance pretension load of 205 kN was applied to M24 bolts with 10.9 grade. In the numerical models for end plate connection, 25 mm thick end plate and 8 M24 bolts 10.9 grade were used. 26 mm bolt holes were drilled.

Modelling fracture of the steel in ABAQUS is enormous and complicated task. Therefore, instead of modeling fracture, rupture indices were used to compare each specimen to determine which one is more susceptible to the fracture.

Three steps were defined in the numerical models. Boundary conditions were defined in the first step of the analysis. The pretension forces of the bolt were given in the second step of the analysis. Loading was applied to the top of the beam in the final step of the analysis. A total of six numerical models including five numerical models for parametric study and a verification model were developed.

### 3.2.1 Element and mesh model

Three dimensional finite element models for the RBS connections were created using eight node brick elements with reduced integration (C3D8R). Four layers of elements were employed through the thickness of the flanges, webs, end plate and beam splice connection in order to simulate buckling and bending accurately. While finer mesh was used for the radius cut, end-plated connection and beam to splice region, coarse mesh was used for the rest of the section. The detailed mesh configurations are given in Fig. 5.

The numerical parametric study was performed by a standard computer with Intel I7 4790 CPUs @3.60 GHZ and 16 GB DDR3 physical ram. The number of elements and nodes, and also computational time of each model are given in Table 4. It should be noted that the computational time of the model includes only the cyclic loading. Time spent for elastic buckling analysis was not included in the computational time. It is also worth mentioning that one of the main reason of high computational time is due to frictional surfaces rather than the number of elements.

### 3.2.2 Interactions and boundary conditions

Modelling proper boundary conditions is very crucial to simulate experiments accurately. The boundary conditions used in the numerical models are shown in Fig. 6. Since the column was not modeled, a part of the column flange where the end plate was connected to the column was introduced to the model in order to simulate the behavior of the end-plated connection and interaction between the end-plated connection and the column. Lower surface of the column flange was restrained with all degree of freedoms, keeping in mind that the column was designed to behave elastic in the experimental setup. To account the effects of the lateral restraining system, the area where the lateral system and the beam coincide was restrained laterally. In the experiments, the loading was applied through the thick plates connected to the top of the beam (Fig. 4(c)). On the other hand, these plates were not included in the model, a rigid body constraint was defined at the end of the beam instead. Cyclic loading protocol according to the AISC provisions (AISC, 2016b) given in Fig. 3 was applied to this rigid body and cyclic loading was applied to the model using displacement controlled loading.

The finite sliding surface to surface contact was used for surface between the beam splice and the bolts, between the beam splice and the beam and between the end-plated connection and column flange. The friction coefficient was taken as 0.3.

### 3.2.3 Geometric Imperfections

Geometric imperfections were introduced to the model in order to trigger the buckling of the RBS connections. To this end, the elastic eigenvalue buckling analyses were performed for each model.

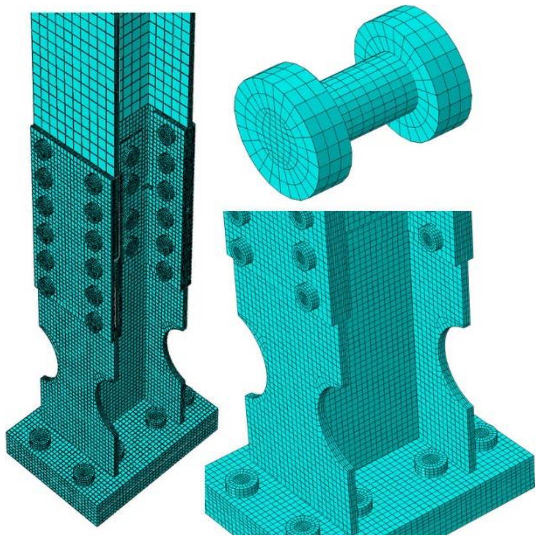

Fig. 5 Mesh configurations

Table 4 Properties of the numerical models

| Model | Number of elements | Number of nodes | Computational Time (hour) |
|---|---|---|---|
| S1 | 93454 | 127512 | 43 |
| S2 | 90418 | 123612 | 41 |
| S3 | 95776 | 130062 | 49 |
| S4 | 94602 | 129082 | 47 |
| S5 | 86084 | 117654 | 32 |

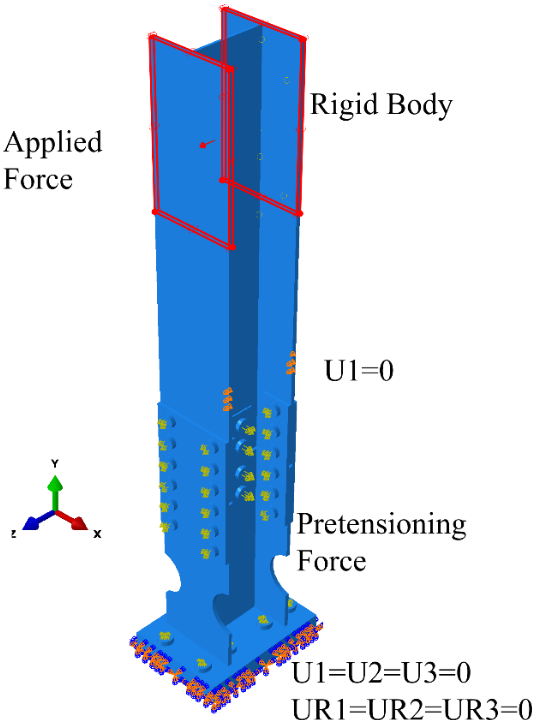


Fig. 6 Boundary conditions

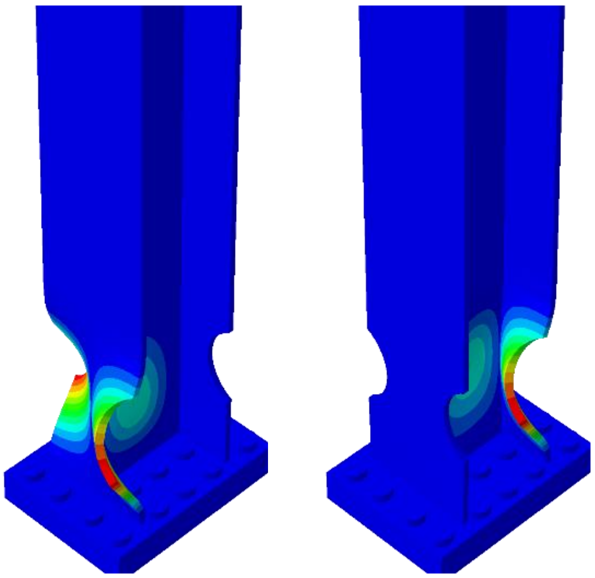

(a) First Mode (b) Second Mode

Fig. 7 Buckling Modes

First two buckling modes were scaled and superposed to simulate adequate geometric imperfection. Fig. 7 demonstrates the first two buckling modes. These imperfections were implemented using "IMPERFECTION" option in ABAQUS. A values of d/150 and $b_f$/150 which are recommended by ASTM (ASTM, 2003) were utilized for local web and flange imperfections, respectively.

### *3.2.4 Material model*

In order to simulate material model, nonlinear isotropic and kinematic hardening material model utilized by Elkady and Lignos (2015) was adapted. Nonlinear isotropic and kinematic hardening parameters were defined using Eqs. (11) and (12).

$$\alpha = \frac{C}{F_y}(\sigma - \alpha)\varepsilon_{pl} - \gamma\alpha\varepsilon_{pl} \tag{11}$$

$$\sigma = F_y + Q_\infty(1 - e^{-b\varepsilon_{pl}}) \tag{12}$$

where $\alpha$ is the backstress, $C$ is the initial kinematic hardening modulus, $F_y$ is yield strength of plate, $\sigma$ is the equivalent yield stress at zero plastic strain, $\varepsilon_{pl}$ is cumulative plastic strain, $\gamma$ is the rate at which $C$ decreases with cumulative plastic strain $\varepsilon_{pl}$, $Q\infty$ is the maximum change in the size of the yield surface and $b$ is the rate at which the size of the yield surface changes as plastic deformation develops.

The material properties of $E$, $F_y$, $C$ and $\gamma$ can be obtained from monotonic tensile test. On the other hand, $Q_\infty$ and $b$ should be determined from cyclic tests. Cyclic tests conducted by Kaufmann *et al.* (2001) and Krawinkler *et al.* (1983) can used to determine these variables. In this study, $C$, $\gamma$, $Q_\infty$ and $b$ are used as 3378 MPa, 20, 90 MPa and 12, respectively assuming that the materials in this study represents ASTM A992 Gr.50. The interested readers can refer to Elkady (2016) for more detail.

### *3.2.5 Verification of numerical model*

In order to substantiate the boundary conditions, material model, mesh configurations and interactions which were assumed to develop the numerical models, the specimen given in the experimental study was simulated. The results of the numerical models were compared to the experimental findings in terms of hysteresis behaviors and deformed shapes. Moment-rotation curve of the verification model is given in Fig. 8, in comparison with the experimental result. Fig. 8(a) compares the numerical and experimental result in full loading protocol while Fig. 8(b) compares only last two cycles which are 0.06 rad and 0.07 rad rotations. The moment was calculated at column face due to the applied load. It can be seen from Fig. 8 that the numerical model was able to simulate the experimental results in terms of the hysteresis behavior. Only 3% difference was observed at maximum moments obtained from the numerical model and experimental findings.

Fig. 9 depicts the progressive damage of the specimen during the experiment. Initial yielding of the flange around the RBS cut was observed at positive excursion of 0.03 (Fig. 9(a)). The yielding was progressed toward the center of the RBS cut at 0.05 rad (Fig. 9(b)). Local buckling of the flange was initiated at 0.06 rad. Excessive flange and web buckling were observed at positive excursion of 0.07 rad (Fig. 9(c)). Due to the limitation of the experimental setup, the experiment was terminated at 0.07 rad. The specimen successfully completed 0.06 rad.

Fig. 10(a) demonstrates PEEQ distribution of the verification model at 0.07 rad. It is seen that maximum PEEQ occurs in the RBS cut as it was expected. Fig. 10(b) and Fig. 10(c) demonstrate buckling shapes of the web and flanges, respectively. When Figs. 10(b) and 10(c) are compared with Fig. 9(c), it is observed that flange and web

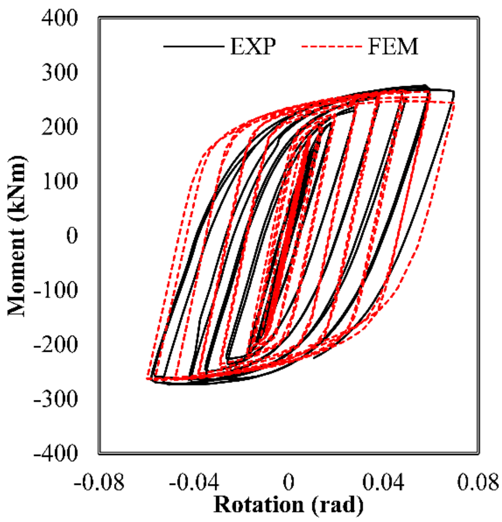


(a) Full loading protocol

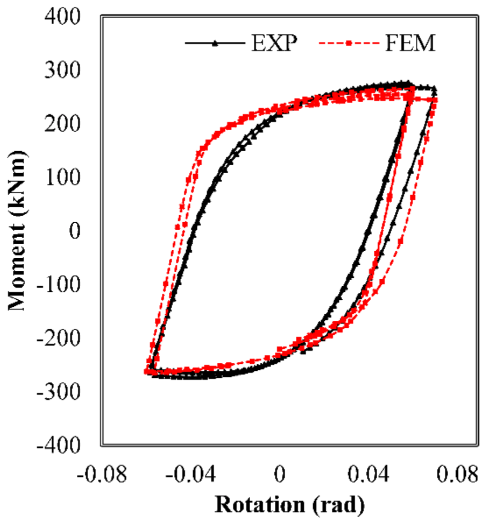


(b) 0.06 and 0.07 rad rotations

Fig. 8 Hysteresis behaviors of the numerical and experimental study

(a) 0.03 rad (b) 0.05 rad (c) 0.07 rad

Fig. 9 Progressive damage

buckling shapes occurred in the experiments are also captured in the verification model. When compared to the hysteresis behaviors and buckling modes, it can be said that a good conformance was captured between the moments at each cycle of the numerical and experimental results.

#### *3.2.6 Response Indices*

Since fracture or crack is not modeled explicitly, the level of potential fracture to be occurred can be determined using response indices. The pressure index, Mises index, tri-axiality index (TI), equivalent plastic strain index (PEEQ) and rupture index (RI) are the most common indices to assess the potential fracture. These indices are defined in Eqs. (13)-(17) (El-Tawil *et al.* 1999). The location where large values of RI are accumulated indicates the location of the greatest potential fracture (Ricles *et al.* 2001). RI can not be used as a criterion for fracture initiation. Instead, it is used to compare different configurations to evaluate which one has the highest potential of the fracture (Bozkurt et al. 2019). The rupture index is used by many researches to evaluate the level of damage to be occurred at the beam-to-column connections (Kim *et al.* 2008, Rahnavard *et al.* 2015, Vatansever and Kutsal 2018, Zhang and Ricles 2006, Hu *et al.* 2014). Rupture index is defined in Eq. (13).

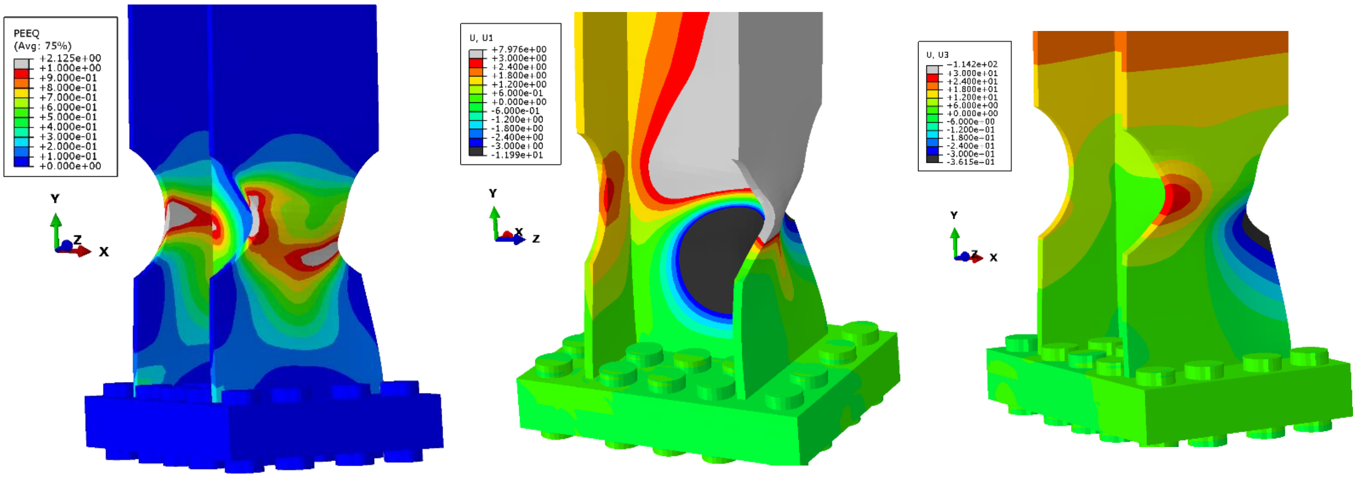


(a) PEEQ distribution (b) Buckling of web (c) Buckling of flange

Fig. 10 PEEQ distribution and the buckling shapes

$$RI = \frac{PEEQ}{\exp\left(-1.5\dfrac{p}{q}\right)} \tag{13}$$

where *PEEQ* is the plastic equivalent strain and calculated as ratio of effective plastic strain to yield strain. *PEEQ* measures local plastic strain demand and higher value of *PEEQ* indicates potential damage and vulnerability. $p$ and $q$ are hydrostatic pressure and von Mises stress, respectively. The calculation of *PEEQ*, $p$ and $q$ are given in Eqs. (14)-(17).

$$PEEQ = \sqrt{\frac{2}{3}\varepsilon_{ij}^{p}\varepsilon_{ij}^{p}} \tag{14}$$

$$p = -\frac{1}{3}tr(\sigma_{ij}) = -\frac{1}{3}\sigma_{ii} \tag{15}$$

$$q = \sqrt{\frac{3}{2}S_{ij}S_{ij}} \tag{16}$$

where $\varepsilon^{p}_{ij}$ stand for the plastic strain in direction i and j, $\sigma_{ij}$ is Cauchy stress and $S_{ij}$ is deviatoric stress.

The ratio of hydrostatic pressure to von Mises stress is called as tri-axiality index (TI). The values between 0.75 and 1.5 can lead to large reduction in rupture strain and the values less than 1.5 can initiate brittle failure (Kim *et al.* 2002). TI is defined in Eq. (17).

$$TI = \frac{p}{q} \tag{17}$$

#### *3.2.7 Details of the numerical models*

The details of the proposed R-RBS connection are given in Table 5. Five numerical models were developed in order to investigate the behavior of the R-RBS connections. The dimensions of the parameter $c$ and $e$, and types of the beam-to-column connection were the parameters studied in this paper. Specimens S1, S2, S3 and S4 represent the R-RBS connection which have both the end-plated connection and the beam splice connection while Specimen S5 represent the typical RBS connection in the column-tree connection which only includes the beam splice connection and other end was welded to the column. One of the aim of this study is to minimize the length of the RBS connection to be replaced after an earthquake. If the RBS connection is damaged, the damaged section can be removed and replaced. Therefore, minimizing the length of the R-RBS connection reduce the repair cost. More importantly is that the weight and length of the replaceable part is quite important since the replacement will be performed inside existing structure where limited hoisting and maneuver can be operated. Pursuant to this goal, the parameters $a$ and $b$ are selected as the minimum value of the AISC recommendations (AISC, 2016a). To this end, for all specimens the parameter $a$ and $b$ were selected as 120 mm and 150, respectively. Additionally, the defined parameter $e$ was selected as 0 to minimize the length of the R-RBS connections and selected as equal to the parameter $a$ to examine the behavior of the R-RBS with different value of the parameter $e$. For Specimens S2 and S4 the parameter $e$ was selected as 0 while the parameter $e$ was selected as 120 mm for Specimens S1, S3 and S5. The parameter $c$ was selected as the maximum and minimum values of the AISC recommendations to show that the proposed R-RBS connection can be used with the AISC recommendations regardless of the selected parameters. Therefore, the parameter $c$ is selected as 60 mm for Specimens S1 and S2 while the parameter $c$ was selected as 25 mm for Specimens S3, S4 and S5.

## **4. Results and discussions**

Five R-RBS connections were analyzed under cyclic

Table 5 The details of the numerical models.

| Models | S1 | S2 | S3 | S4 | S5 |
|---|---|---|---|---|---|
| Mesh Configuration | 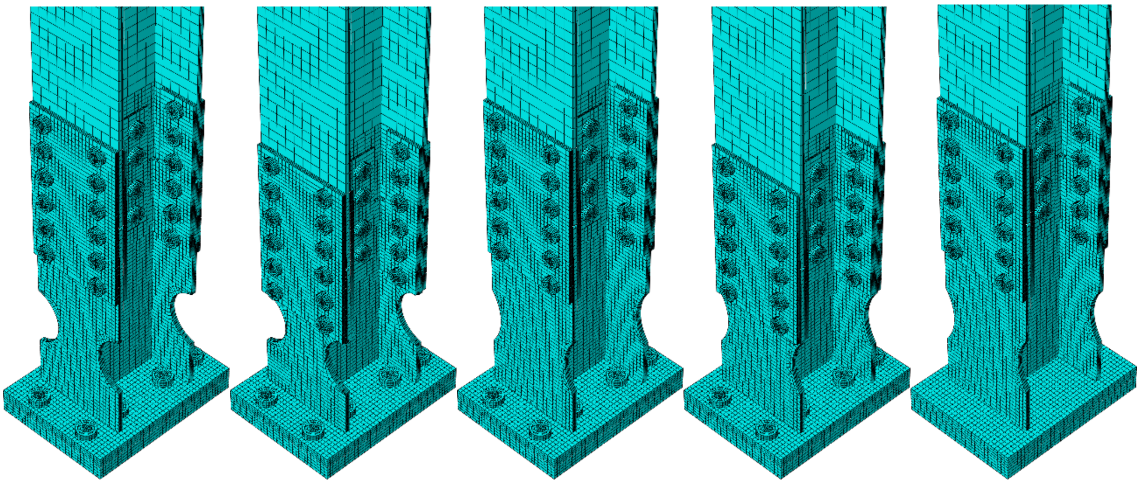 | | | | |
| Beam-to-column Connection | Bolted | Bolted | Bolted | Bolted | Welded |
| Beam Splice Connection | Yes | Yes | Yes | Yes | Yes |
| a (mm) | 120 | 120 | 120 | 120 | 120 |
| b (mm) | 150 | 150 | 150 | 150 | 150 |
| c (mm) | 60 | 60 | 25 | 25 | 25 |
| R (mm) | 76.5 | 76.5 | 129 | 129 | 129 |
| e (mm) | 120 | 0 | 120 | 0 | 120 |

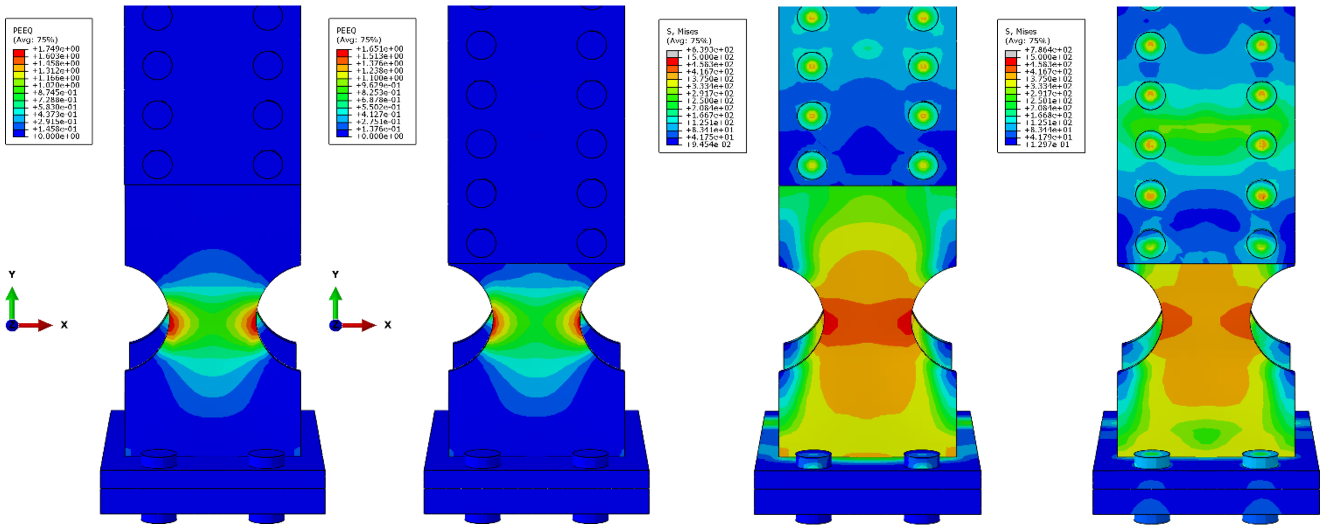

(a) PEEQ distrubition of Specimen S1 (b) PEEQ distrubition of Specimen S2 (c) Von Mises Stress distrubition of Specimen S1 (d) Von Mises Stress distrubition of Specimen S2

Fig. 11 PEEQ and Von Mises Stress Distributions of Specimens S1 and S2

loading according to the AISC loading protocol. The same section profiles and material models were used in all the numerical models. Von Mises stress and PEEQ distribution of the RBS connections at 0.06 rad rotation are given in Figs. 11-13.

As seen in Figs. 11-13, local buckling was observed in the flanges. No plastic strain was observed at the beam splice connection, revealing that it will be reusable after the RBS connection gets damaged. As expected, increasing the parameter c leads to accumulated stresses at the reduced section.

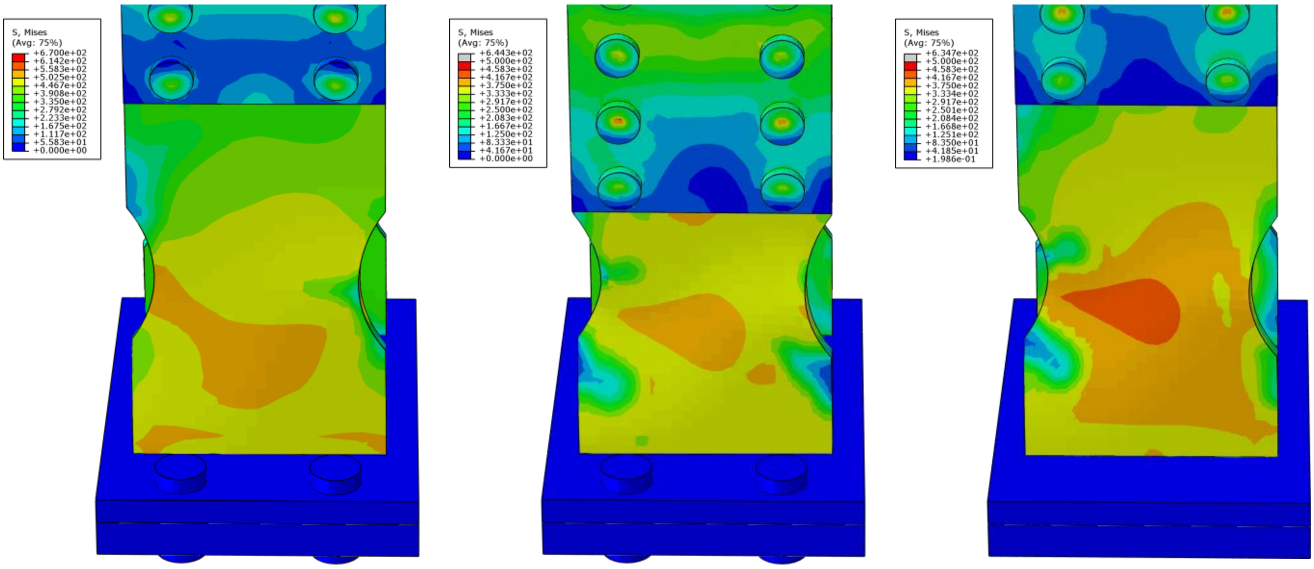

(a) For Specimen S3 (b) For Specimen S4 (c) For Specimen S5

Fig. 12 Von Mises Stress Distributions of Specimens S3, S4 and S5

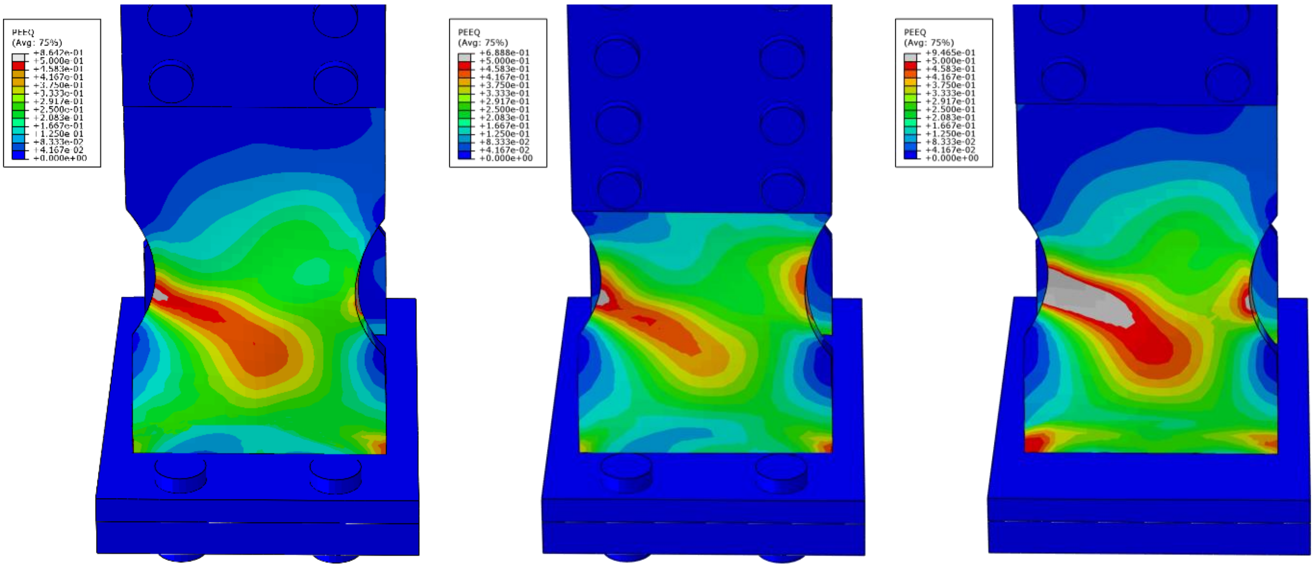

(a) For Specimen S3 (b) For Specimen S4 (c) For Specimen S5

Fig. 13 PEEQ Distributions of Specimens S3, S4 and S5

To make a fair comparison, the specimens having the same value of the parameter *c* are compared with each other. When Fig. 11 is examined, slightly higher *PEEQ* values are observed at Specimen S1. Moreover, the stresses observed at the reduced cut section, and at the interface of the RBS flange and the end-plate are higher than those of Specimen S2. For these specimens, the buckling shape of the flange is quite similar. Investigating Figs. 12 and 13, it is observed that the buckling shapes of Specimens S3, S4 and S5 are similar. In these specimens, higher *PEEQ* values are observed at the edge of the radius cut. The maximum *PEEQ* value is observed at Specimen S5, which represents the typical column-tree connection with RBS connection.

Comparing Specimens S3 and S4, it is seen that slightly higher *PEEQ* values are observed at Specimen S3. Moreover, higher stresses are observed at the reduced cut and the interface of the RBS flange and the end-plate at Specimen S5, compared to Specimens S3 and S4.

For all specimens, no plastic deformation was observed at the end-plated bolted connection. Moreover, no yielding was observed at the connecting bolts. These results indicate that the design of the end-plated connection can be considered sufficiently safe.

The hysteresis behavior of the specimens is presented in Fig. 14. The analyses were conducted up to a 0.06 rad rotation. A slight strength degradation due to the local buckling of the flange was observed in Specimens S1 and

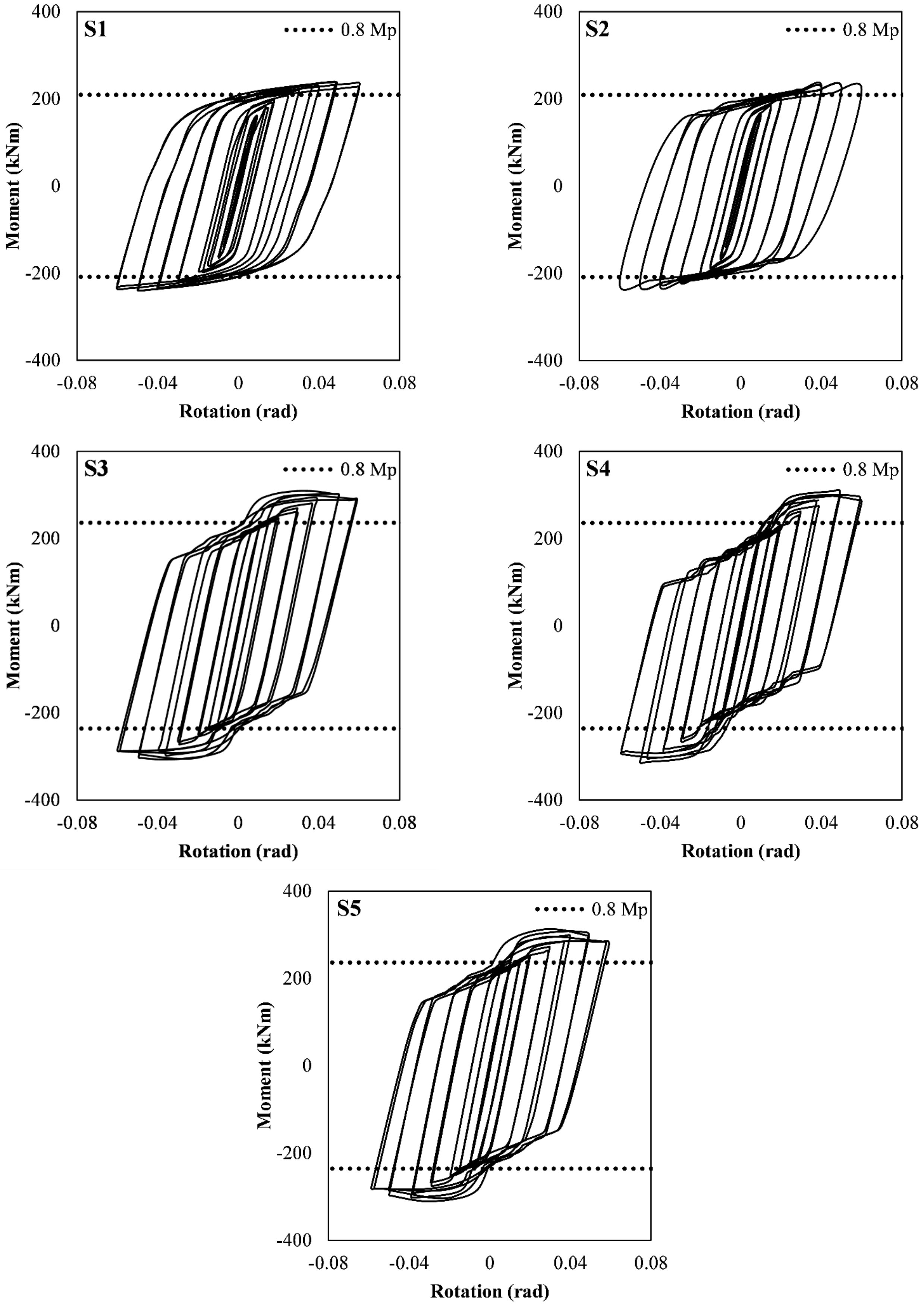


Fig. 14 Hysteresis loops of the specimens

S2 while Specimens S3, S4 and S5 exhibited slightly higher strength degradation than those of Specimens S1 and S2. During the analyses, if the moment of the specimen does not drop below 80% of the moment capacity of the beam, it is accepted that the specimen achieved a 0.06 rad rotation before failure. However, the rotation value at which the moment drops below 80% of the moment capacity is accepted as the rotation capacity of the beam.

Table 6 demonstrates the rotation capacity, the maximum moment and the energy dissipation capacity of the specimens. Energy dissipation capacity was calculated as the total area enclosed by the hysteresis loops up to 0.06 rad rotation. Specimen S3 exhibited the highest strength degradation and the moment declined 5% at 0.06 rad rotation. Specimens S1 and S2 achieved almost the equal energy dissipation capacities, whereas, Specimens S3, S4 and S5 showed similar energy dissipation capacities. All specimens successfully completed a 0.06 rad rotation. The moment capacities of Specimens S1 and S2 were less than those of other specimens since the parameter *c* used at specimens S1 and S2 are larger than those of the other specimens. As expected, increasing the trimming area resulted in a significant reduction in the moment capacity of the RBS connection.

To make a fair comparison, the effect of the parameter *e* is investigated for Specimens S1 and S2, and Specimens S3 and S4, where the parameter *c* is equal in each groups of specimens. It is obtained that decreasing the parameter *e* results in no significant change in the energy dissipation and moment capacities of the RBS connection. Moreover, when the results of Specimens S3 and S5 are compared, no significant difference is observed in the moment capacity and energy dissipation capacities.

Table 6 Summary of the results

| Model | Rotation Capacity (rad) | Maximum Moment (kNm) | Energy Dissipation Capacity (MJ) |
|---|---|---|---|
| S1 | 0.6 | 238 | 209 |
| S2 | 0.6 | 236 | 212 |
| S3 | 0.6 | 309 | 258 |
| S4 | 0.6 | 316 | 251 |
| S5 | 0.6 | 310 | 255 |

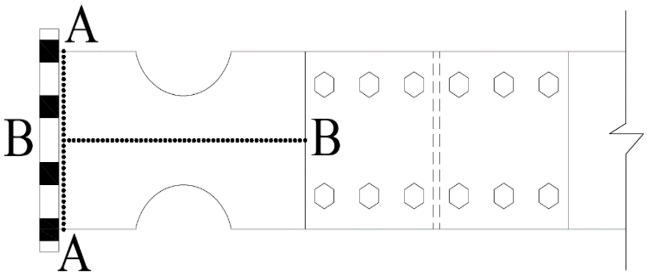

Fig. 15 Paths in which response indices computed

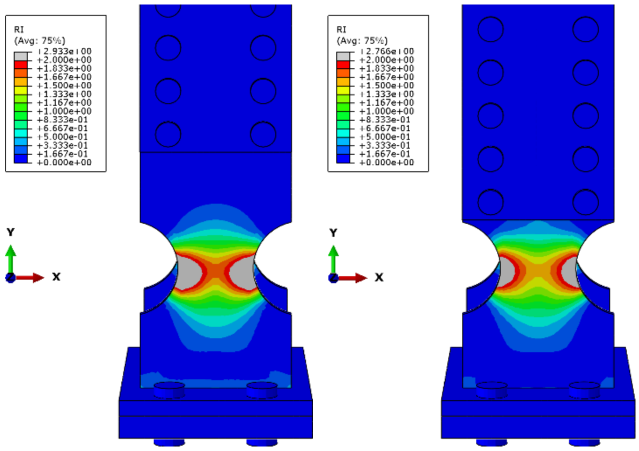
(a) Specimen S1 (a) Specimen S2

Fig. 16 RI contours of Specimens S1 and S2

The rupture index was calculated along the two paths on the surface of top flange as shown in Fig. 15. Path A is the line drawn along the flange width parallel to the end-plate and Path B is the line drawn from the end-plate face to the beam splice connection. The Rupture Index, PEEQ and Tri-axiality index are compared for 0.06 rad rotation for all specimens and the results are presented in Fig. 17.

It is seen from Figs. 17(a)-17(c) that Specimen S5 exhibited higher PEEQ and RI values along the Path A when compared to those of other specimens. Considering the Path A, the specimen S5 experienced the highest TI among other specimens (Fig. 17(b)) which indicates that the specimen S5 is more prone to brittle failure compared to the other specimens along Path A. The lowest RI and PEEQ values are observed at Specimen S2. RI and PEEQ values of Specimen S2 is lower than that of specimen S1, and RI and PEEQ values of Specimen S3 is lower than that of Specimen S4. These results indicated that the specimens with lower value of the parameter *e* are less prone to brittle failure along Path A. This can be seen also from Fig. 16 which compares RI contours of Specimens S1 and S2 at 0.06 rad rotation. It is clearly seen in Fig. 16 that Specimen S1 exhibited higher value of RI along Path A. Moreover, there is a general trend that plastic demands occurred at edges of the top flange was higher than that of middle portion along Path A.

When the RI values of Specimens S1 and S2 are compared, it is seen that the contours of RI are similar (Fig. 16). In both cases, the maximum RI value was occurred at the reduced section. Furthermore, the maximum values of RI observed at Specimens S1 and S2 were also quite similar. However, it can be said that Specimen S1 is slightly more prone to the failure at rotation 0.06 rad around the reduced cut. These results indicated that the use of the parameter *e* equal to 0 is reasonable since only the difference between these specimens is the value of the parameter *e*.

As it was expected, Specimens S1 and S2 showed higher RI and PEEQ values than other specimens along Path B (Fig. 17(d)-17(f)) since the parameter *c* was higher in Specimens S1 and S2 which can reduce moment capacity significantly. Specimen S5 exhibited higher PEEQ and RI

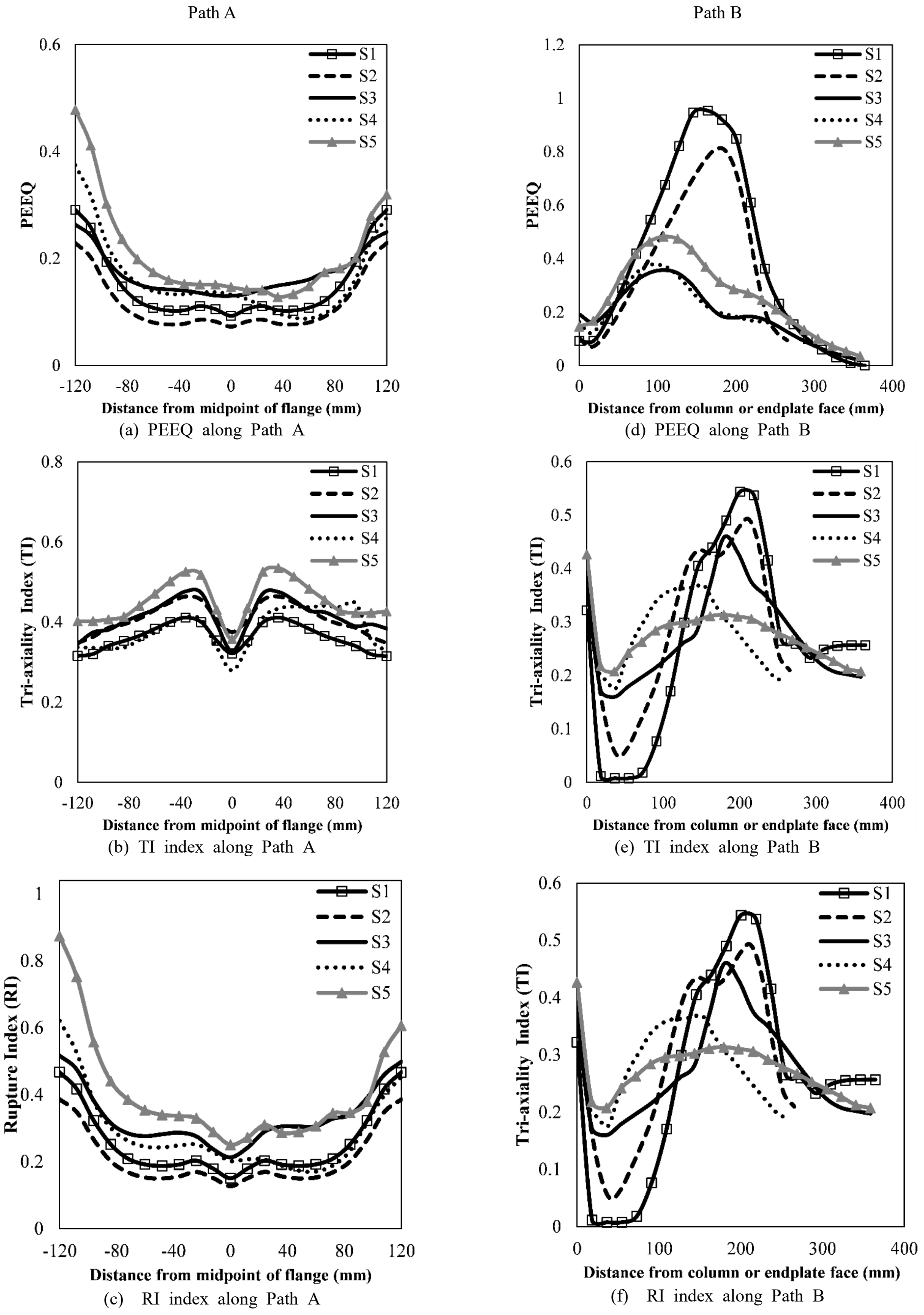


Fig. 17 Response indices along Path A and B

values compared to other specimens which have same value of the parameter *c* along Path B. The values of RI and PEEQ decrease after the reduced section and almost no RI and PEEQ values were observed at edge of the beam splice connection. For all specimens, the highest PEEQ and RI values were observed in the reduced section. Along Path B up to 120 mm, which is equal to the parameter *a*, the values of TI for all specimens are very low (Fig. 17(e)) which indicate that the occurrence of damage up to 120 mm is very unlikely.

## 5. Conclusions

The main purpose of this study is to develop optimum, practical and valid connection which enables:

- to facilitate assembly and construction
- to eliminate welding processes during replacement of the damaged RBS connection
- to enhance behavior of reduced beam section
- to facilitate replacement of reduce beam section after earthquake

Pursuant to this goal, the R-RBS connection is proposed. The proposed connection is examined under cyclic loading according to the AISC seismic provision. Experimental and numerical analyses have been undertaken to investigate the cyclic performance of the proposed connection. Numerical models were developed in order to explore the optimum design of the R-RBS connections. The nonlinear finite element results were compared in terms of the moment capacity, energy absorption capacity, rupture index, tri-axiality index and PEEQ. Following results can be drawn from this present study:

- A good agreement is observed between numerical results and experimental findings. The numerical model captured both hysteresis behavior and failure modes.
- The results revealed that the R-RBS connections perform excellent seismic behavior under cyclic loading and the proposed connection satisfies the AISC criteria.
- Higher RI and PEEQ are observed at the interface of the RBS flange and the end-plate. However, these values are much lower than the RI and PEEQ values observed at the reduced section. Therefore, the failure is expected to occur at the reduced section rather than the interface of the RBS flange and the end-plate.
- The fact that very low TI is observed at the end-plate face to the reduced section, which is equal to the parameter *a*, indicates the potential damage to be occurred within the distance of the parameter *a* is very unlikely.
- A general trend is observed that RI and PEEQ values decrease from the reduced section to the beam splice. Almost no RI and PEEQ values are observed at the beam splice connection. These results indicate that the beam splice connection can be reusable after an earthquake.
- The proposed R-RBS connection exhibited similar performance in terms of the moment and energy dissipation capacity and buckling modes with the typical RBS connection.
- The shortest replaceable RBS connection are slightly less prone to failure when compared the longer R-RBS connections. Therefore, selecting the smallest values of the parameters *a* and *b* recommended in the AISC provision are recommended. Moreover, connecting the beam splice connection adjacent to the radius cut, in other words selecting the parameter *e* equal to 0 is recommended.
- The presented design of the end-plated connection can be safely used for the R-RBS connection. Moreover, the beam splice connection should be designed to be stronger than the capacity of RBS connection.

Following studies are aimed for future studies:

- Experimental studies are going to be conducted by Author at Necmettin Erbakan University in order to qualify the R-RBS connection.
- Developing a valid connection which can be replaceable up to 0.5% residual drift is aimed.
- In order to investigate performance of the proposed connection for deeper sections and narrow flange sections, additional studies should be conducted.

## Acknowledgments

This study has been supported by the Department of Scientific Research Projects at Necmettin Erbakan University with the project coded 181219006.

## References

Aghaei, M., Forouzan, M.R., Nikforouz, M. and Shahabi, E. (2015), "A study on different failure criteria to predict damage in glass/polyester composite beams under low velocity impact", *Steel Compos. Struct.*, **18**(5), 1291-1303. https://doi.org/10.12989/scs.2015.18.5.1291.

AISC (2016a), AISC 341-16, *Seismic Provisions for Structural Steel Buildings*, American Institute of Steel Construction, Chicago, IL, USA

AISC (2016b), AISC 358-16, P*requalified Connections for Special and Intermediate Steel Moment Frames for Seismic Applications*, American Institute of Steel Construction, Chicago, IL, USA

AISC (2016c), AISC 360-16, *Specification for Structural Steel Buildings*, American Institute of Steel Construction, Chicago, IL, USA

Akrami, V. and Erfani, S. (2015), "Effect of local web buckling on the cyclic behavior of reduced web beam sections (RWBS)", *Steel Compos. Struct.*, **18**(3), 641-657. https://doi.org/10.12989/scs.2015.18.3.641.

Ashakul, A. and Khampa, K. (2014), "Effect of plate properties on shear strength of bolt group in single plate connection", *Steel Compos. Struct.*, **16**(6), 611-637. https://doi.org/10.12989/scs.2014.16.6.611.

Atashzaban, A., Hajirasouliha, I., Jazany, R.A. and Izadinia, M. (2015), "Optimum drilled flange moment resisting connections for seismic regions", *J. Constr. Steel Res.*, **112**, 325-338. https://doi.org/10.1016/j.jcsr.2015.05.013.

Balut, N. and Gioncu, V. (2003), *Suggestion for an improved 'dog-bone'solution*, Proc., Stessa, 129-134.

Bozkurt, M.B., Kazemzadeh Azad, S. and Topkaya, C. (2019), "Development of detachable replaceable links for eccentrically braced frames", *Earthq. Eng. Struct. D.*, **48**(10), 1134-1155. https://doi.org/10.1002/eqe.3181.

Bozkurt, M.B. and Topkaya, C. (2017), "Replaceable links with direct brace attachments for eccentrically braced frames", *Earthq. Eng. Struct. D.*, **46**(13), 2121-2139. https://doi.org/10.1002/eqe.2896.

Bozkurt, M.B. and Topkaya, C. (2018), "Replaceable links with gusseted brace joints for eccentrically braced frames", *Soil Dynam. Earthq. Eng.*, **115**, 305-318. https://doi.org/10.1016/j.soildyn.2018.08.035.

Chegenizadeh, A., Ghadimi, B., Nikraz, H. and Simsek, M. (2014), "A novel two-dimensional approach to modelling functionally graded beams resting on a soil medium", *Struct. Eng. Mech.*, **51**(5), 727-741. https://doi.org/10.12989/sem.2014.51.5.727.

Dere, Y. (2016), "Assessing a retrofitting method for existing RC buildings with low seismic capacity in Turkey", *J. Perform. Constr. Fac.*, **31**(2), 04016098. https://doi.org/10.1061/(ASCE)CF.1943-5509.0000969.

Ding, F., Tan, L., Liu, X. and Wang, L. (2017), "Behavior of circular thin-walled steel tube confined concrete stub columns", *Steel Compos. Struct.*, **23**(2), 229-238. https://doi.org/10.12989/scs.2017.23.2.229.

Dubina D., Stratan A. and Dinu F. (2008), "Dual high-strength steel eccentrically braced frames with removable links", *Earthq. Eng. Struct. D.*, **37**(15), 1703-1720. https://doi.org/10.1002/eqe.828.

Elkady, A. (2016), "Collapse risk assessment of steel moment resisting frames designed with deep wide-flange columns in seismic regions", Ph.D. dissertation, McGill University.

Elkady, A. and Lignos, D.G. (2015), "Analytical investigation of the cyclic behavior and plastic hinge formation in deep wide-flange steel beam-columns", *Bull. Earthq. Eng.*, **13**(4), 1097-1118. https://doi.org/10.1007/s10518-014-9640-y.

El-Tawil, S., Vidarsson, E., Mikesell, T. and Kunnath, S.K. (1999), "Inelastic behavior and design of steel panel zones", *J. Struct. Eng.*, **125**(2), 183-193. https://doi.org/10.1061/(ASCE)0733-9445(1999)125:2(183).

Eom, S.S., Vu, Q.V., Choi, J.H., Papazafeiropoulos, G. and Kim, S.E. (2019), "Behavior of composite CFST beam-steel column joints", *Steel Compos. Struct.*, **32**(5), 583-594. https://doi.org/10.12989/scs.2019.32.5.583.

Garoosi, A.M., TahamouliRoudsari, M. and Hashemi, B.H. (2018). "Experimental evaluation of rigid connection with reduced section and replaceable fuse", *Structures*, **16**, 390-404. https://doi.org/10.1016/j.istruc.2018.11.010.

Hu, F., Shi, G., Bai, Y. and Shi, Y. (2014), "Seismic performance of prefabricated steel beam-to-column connections", *J. Constr. Steel Res.*, **102**, 204-216. https://doi.org/10.1016/j.jcsr.2014.07.012.

Kantar, E. and Anil, O. (2012), "Low velocity impact behavior of concrete beam strengthened with CFRP strip", *Steel Compos. Struct.*, **12**(3), 207-230. https://doi.org/10.12989/scs.2012.12.3.207.

Kaufmann E.J., Metrovich B.R. and Pense A.W. (2001), "Characterization of cyclic inelastic strain behavior on properties of A572 Gr. 50 and A913 Gr. 50 rolled sections, ATLSS Report 01–13", National Center for Engineering Research on Advanced Technology for Large Structural Systems, Bethlehem

Kazemzadeh Azad, S. and Topkaya, C. (2017), "A review of research on steel eccentrically braced frames", *J. Constr. Steel Res.*, **128**, 53-73. https://doi.org/10.1016/j.jcsr.2016.07.032.

Kazemzadeh Azad, S. and Uy, B. (2020), "Effect of concrete infill on local buckling capacity of circular tubes", *J. Constr. Steel Res.*, **165**, 105899. https://doi.org/10.1016/j.jcsr.2019.105899.

Kim, T., Whittaker, A.S., Gilani, A.S.J., Bertero, V.V. and Takhirov, S.M. (2002), "Cover-plate and flange-plate steel moment-resisting connections", *J. Struct. Eng.,* **128**(4), 474-482. https://doi.org/10.1061/(ASCE)0733-9445(2002)128:4(474).

Kim, Y.J., Shin, K.J. and Kim, W.J. (2008), "Effect of stiffener details on behavior of CFT column-to-beam connections", *Int. J. Steel Struct.*, **8**(2), 119-133.

Kota, S.K., Rama, J.S. and Murthy, A.R. (2019), "Strengthening RC frames subjected to lateral load with Ultra High-Performance fiber reinforced concrete using damage plasticity model", *Earthq. Struct.*, **17**(2), 221-232. https://doi.org/10.12989/eas.2019.17.2.221.

Krawinkler, H., Zohrei, M., Lashkari-Irvani, B., Cofie, N.G. and Hadidi-Tamjed, H. (1983), "Recommendations for experimental studies on the seismic behavior of steel components and materials, Report No. 61", The John A. Blume Earthquake Engineering Center, Stanford University, Stanford

Lopez-Arancibia, A., Altuna-Zugasti, A.M., Aldasoro, H.A. and Pradera-Mallabiabarrena, A. (2015), "Bolted joints for single-layer structures: numerical analysis of the bending behaviour", *Struct. Eng. Mech.*, **56**(3), 355-367. https://doi.org/10.12989/sem.2015.56.3.355.

Madenci, E., Özkılıç, Y.O. and Gemi, L. (2020), "Experimental and theoretical investigation on flexure performance of pultruded GFRP composite beams with damage analyses", *Compos. Struct.*, **242**, 112162. https://doi.org/10.1016/j.compstruct.2020.112162.

Mahmoudi, F., Dolatshahi, K.M., Mahsuli, M., Nikoukalam, M.T., and Shahmohammadi, A. (2019), "Experimental study of steel moment resisting frames with shear link", *J. Constr. Steel Res.*, **154**, 197-208. https://doi.org/10.1016/j.jcsr.2018.11.027.

Mansour N., Christopoulos C. and Tremblay R. (2011). "Experimental validation of replaceable shear links for eccentrically braced steel frames", *J. Struct. Eng.*, **137**(10) 1141-1152. https://doi.org/10.1061/(ASCE)ST.1943-541X.0000350.

Mao, C., Ricles, J., Lu, L.W. and Fisher, J. (2001), "Effect of local details on ductility of welded moment connections", *J. Struct. Eng.*, **127**(9), 1036-1044. https://doi.org/10.1061/(ASCE)0733-9445(2001)127:9(1036).

Metwally, I.M. (2014), "Three-dimensional finite element analysis of reinforced concrete slabs strengthened with epoxy-bonded steel plates", *Adv. Concrete Constr.*, **2**(2), 91-108. ttps://doi.org/10.12989/acc.2014.2.2.091.

Momenzadeh, S., Kazemi, M.T. and Asl, M.H. (2017), "Seismic performance of reduced web section moment connections", *Int. J. Steel Struct.*, **17**(2), 413-425. https://doi.org/10.1007/s13296-017-6004-x.

Morshedi, M.A., Dolatshahi, K.M. and Maleki, S. (2017), "Double reduced beam section connection", *J. Constr. Steel Res.*, **138**, 283-297. ttps://doi.org/10.1016/j.jcsr.2017.07.013.

Murray, T.M. and Sumner, E.A. (2003), "Steel Design Guide Series 4 Extended end-plate moment connections seismic and wind applications", American Institute of Steel Construction.

Nikoukalam, M.T. and Dolatshahi, K.M. (2015), "Development of structural shear fuse in moment resisting frames", *J. Constr. Steel Res.*, **114**, 349-361. https://doi.org/10.1016/j.jcsr.2015.08.008.

Oh, K., Lee, K., Chen, L., Hong, S. and Yang, Y. (2015), "Seismic performance evaluation of weak axis column-tree moment connections with reduced beam section", *J. Constr. Steel Res.*, **105**, 28-38. https://doi.org/10.1016/j.jcsr.2014.10.005.

Oh, K., Li, R., Chen, L., Hong, S.B. and Lee, K. (2014), "Cyclic testing of steel column-tree moment connections with weakened beam splices", *Int. J. Steel Struct.*, **14**(3), 471-478. https://doi.org/10.1007/s13296-014-3004-y.

Oh, K., So, J., Ha, H. and Lee, K. (2016), "Seismic performance evaluation of Korean column-tree steel moment connections", *Int. J. Steel Struct.*, **16**(4), 1287-1298. https://doi.org/10.1007/s13296-016-0089-5.

Özkılıç, Y.O. (2019), "Numerical study of replaceable reduced beam section with beam splice connection", *Proceedings of the*

*8th Internatİonal Steel Structures Symposium*, Konya, Turkey, October.

Özkılıç, Y.O., Madenci, E. and Gemi, L. (2020), "Tensile and compressive behaviors of the pultruded GRFP lamina", *Turkish J. Eng.*, **4**(4), 169-175.

Pachoumis, D.T., Galoussis, E.G., Kalfas, C.N. and Christitsas, A. D. (2009), "Reduced beam section moment connections subjected to cyclic loading : Experimental analysis and FEM simulation", *Eng. Struct.*, **31**(1), 216-223. https://doi.org/10.1016/j.engstruct.2008.08.007.

Pachoumis, D.T., Galoussis, E.G., Kalfas, C.N. and Efthimiou, I.Z. (2010), "Cyclic performance of steel moment-resisting connections with reduced beam sections - experimental analysis and finite element model simulation", *Eng. Struct.*, **32**(9), 2683-2692. https://doi.org/10.1016/j.engstruct.2010.04.038.

Pantò, B., Giresini, L., Sassu, M. and Calio, I. (2017), "Non-linear modeling of masonry churches through a discrete macro-element approach", *Earthq. Struct.*, **12**(2), 223-236. https://doi.org/10.12989/eas.2017.12.2.223.

Plumier, A. (1997), "The dogbone: back to the future", *Engineering Journal-American Institute of Steel Construction*, American Institute Of Steel Construction, Inc., **34**, 61-67.

Rahnavard, R., Hassanipour, A. and Siahpolo, N. (2015), "Analytical study on new types of reduced beam section moment connections affecting cyclic behavior", *Case Studies in Structural Engineering*, **3**, 33-51. https://doi.org/10.1016/j.csse.2015.03.001.

Richards, P. (2019), "A repairable connection for earthquake-resisting moment frames", *Steel Constr.*, **12**(3), 191-197. https://doi.org/10.1002/stco.201900015.

Roudsari, M.T., Abdollahi, F., Salimi, H., Azizi, S. and Khosravi, A.R. (2015), "The effect of stiffener on behavior of reduced beam section connections in steel moment-resisting frames", *Int. J. Steel Struct.*, **15**(4), 827-834. https://doi.org/10.1007/s13296-015-1205-7.

Saleh, A., Zahrai, S.M. and Mirghaderi, S.R. (2016), "Experimental study on innovative tubular web RBS connections in steel MRFs with typical shallow beams", *Struct. Eng. Mech.*, **57**(5), 785-808. http://dx.doi.org/10.12989/sem.2016.57.5.785

.Shen, Y. (2009), "Seismic performance of steel moment-resisting frames with nonlinear replaceable links", Ph.D. dissertation.

Shen, Y., Christopoulos, C., Mansour, N. and Tremblay, R. (2010), "Seismic design and performance of steel moment-resisting frames with nonlinear replaceable links", *J. Struct. Eng.*, **137**(10), 1107-1117. https://doi.org/10.1061/(ASCE)ST.1943-541X.0000359.

Sofias, C.E., Kalfas, C.N. and Pachoumis, D.T. (2014), "Experimental and FEM analysis of reduced beam section moment endplate connections under cyclic loading", *Eng. Struct.*, **59**, 320-329. https://doi.org/10.1016/j.engstruct.2013.11.010.

Song, Y., Uy, B. and Wang, J. (2019), "Numerical analysis of stainless steel-concrete composite beam-to-column joints with bolted flush endplates", *Steel Compos. Struct.*, **33**(1), 143-162. https://doi.org/10.12989/scs.2019.33.1.143.

Sophianopoulos, D.S. and Der, A.E. (2011). "Parameters affecting response and design of steel moment frame reduced beam section connections: An overview", *Int. J. Steel Struct.*, **11**(2), 133-144. https://doi.org/10.1007/s13296-011-2003-5.

Stratan A. and Dubina D. (2004), "Bolted links for eccentrically braced steel frames", *Proceedings of the 5th AISC/ECCS International Workshop: Connections in Steel Structures V. Behaviour*, Strength and Design, Delft, The Netherlands, pp. 223-332.

Swati, A.K. and Gaurang, V. (2014), "Study of steel moment connection with and without reduced beam section", *Case Studies in Structural Engineering*, **1**(1), 26-31. https://doi.org/10.1016/j.csse.2014.04.001.

Tahamouli Roudsari, M., Jamshidi K.H. and Zangeneh, M.M. (2018), "Experimental and numerical investigation of IPE reduced beam sections with diagonal web stiffeners", *J. Earthq. Eng.*, **22**(4), 533-552. https://doi.org/10.1080/13632469.2016.1234422.

Vatansever, C. and Kutsal, K. (2018), "Effect of bolted splice within the plastic hinge zone on beam-to-column connection behavior", *Steel Compos. Struct.*, **28**(6), 767-778. https://doi.org/10.12989/scs.2018.28.6.767.

Wang, M., Shi, Y. and Wang, Y. (2015). "Application of steel equivalent constitutive model for predicting seismic behavior of steel frame", *Steel Compos. Struct.*, **19**(5), 1055-1075. https://doi.org/10.12989/scs.2015.19.5.1055.

Xu, Y., Lu, L. and Zheng, H. (2018), "Parametric study of weak-axis beam-to-column composite connections with asymmetrical reduced beam section", *Int. J. Steel Struct.*, Korean Society of Steel Construction, (0123456789).

Zahrai, S.M., Mirghaderi, S.R. and Saleh, A. (2017a), "Increasing plastic hinge length using two pipes in a proposed web reduced beam section, an experimental and numerical study", *Steel Compos. Struct.*, **23**(4), 421-433. https://doi.org/10.12989/scs.2017.23.4.421.

Zahrai, S.M., Mirghaderi, S.R. and Saleh, A. (2017b), "Tubular Web Reduced Beam Section (TW-RBS) connection, a numerical and experimental study and result comparison", *Steel Compos. Struct.*, **23**(5), 571-583. https://doi.org/10.12989/scs.2017.23.5.571

Zareia, A., Vaghefi, M. and Fiouz, A.R. (2016), "Numerical investigation seismic performance of rigid skewed beam-to-column connection with reduced beam section", *Struct. Eng. Mech.*, **57**(3), 507-528. https://doi.org/10.12989/sem.2016.57.3.507.

Zhang, X. and Ricles, J.M. (2006), "Seismic behavior of reduced beam section moment connections to deep columns", *J. Struct. Eng.*, **132**(3), 358-367. https://doi.org/10.1061/(ASCE)0733-9445(2006)132:3(358).

*CC*